Egypt. J. Chem. **Vol. 68**, No.2 pp. 493 - 505 (2025)

Egyptian Journal of Chemistry

http://ejchem.journals.ekb.eg/

Yellow Oleander Extract as Green Sustainable Corrosion Inhibitor for Aluminum in Hydrochloric Acid Solution

A.S. Fouda*[a], S.H. Etaiw[b], E.S. El-Hussieny[a]

[a]*Department of Chemistry, Faculty of Science, Mansoura University, Mansoura-35516, Egypt*
[b]*Department of Chemistry, Faculty of Science, Tanta University, Tanta, Egypt*

Abstract

Through this study, the use of yellow oleander extract (YOE) as an environmentally friendly and sustainable corrosion inhibitor for Al in 1 M HCl solution was investigated by "mass loss (ML)" method, electrochemical frequency modulation (EFM), electrochemical impedance spectroscopy (EIS) and potentiodynamic polarization (PDP) techniques". The surface analysis of Al has also been studied using scanning electron microscopy (SEM), energy dispersive X-ray spectroscopic (EDX) and atomic force microscopy (AFM) techniques. The obvious impact of temperature on corrosion, with and without YOE was explored inside the temperature assortments of 25ºC till 45 ºC by using ML procedure. PDP data revealed that YOE is considered mixed type inhibitor. Inhibition efficiency (% IE) increases as YOE improves and decreases as temperature increases. The adsorption of YOE on the Al surface follows the Langmuir adsorption isotherm and is considered a physical adsorption. Results obtained using chemical and electrochemical strategies are in good agreement.

Keywords: Corrosion inhibition, Aluminum, Yellow Oleander, HCl, Langmuir isotherm

1. Introduction

Aluminum and its amalgam are important construction materials due to their unique and advanced data as well as a wide variety of mechanical applications, especially in aircraft, cars and nuclear equipment. Al is used in many applications because of its excellent properties, including good mechanical properties, light weight, high electrical conductivity, and corrosion resistance [1]. The most well-known acid inhibitors are organic compounds containing nitrogen, sulphur and oxygen atoms and have a strong inhibitory effect [2-5]. Heterocyclic compounds are used to inhibit the corrosion of iron [6-9], copper [10], aluminium [11-13] and various metals [14, 15] in various corrosive environments. However, many of these compounds have high blocking activity, and some of them can cause unwanted side effects even at very low concentrations due to their toxicity to the human body, adverse environmental and market impacts, and high prices [16]. Plant extracts are inexpensive and environmentally safe, which is why they are acting as environmentally friendly and naturally inhibitor for corrosion. Lately, So many plant extracts have been used as useful corrosion inhibitors for Al alloys dipped in HCl solution, like garlic [17], blackberry [18], Guinea Piper seeds [19], , red onion peel [20]. The inhibitory ability of these extracts is often related to the presence of organic substances containing tannins, alkaloids and nitrogenous bases, carbohydrates, and proteins in their composition. These compounds often include polar functionalities with N, O, or S atoms and have double or triple bonds conjugated to aromatic rings in their molecular structure, which are important adsorption centres. The Yellow Oleander plant is the Apocynaceae YOE family. The Latin name for YOE is Cascabela thevetia. This plant is native of South & Central America. It contains a milky sap holds a compound called thevetin which is used as a heart stimulant, but it is extremely poisonous in its natural form, as are all parts of the plants, especially the seeds. The toxins are cardenolides called Thevetin B and Thevetin A (Cerebroside), others include neriifolin, peruvoside, thevetoxin and ruvoside. The plant's toxins have been tested in experiments for uses in biological pest control [21]. This study aimed to show the inhibitory properties of YOE and investigate the corrosion resistance using ML, PDP, EIS and EFM measurements. AFM and SEM are used for surface analyses. The influence of temperature on corrosion rate and thermodynamic parameters was determined and discussed.

2. Experimental Methods

2.1. Materials and Solutions

Investigation performed to study the corrosion behavior of aluminum (Al) using specimens containing specific elements: 0.3% silicon, 0.6% iron (Fe), 0.1% copper, 1.4% manganese, 0.05% chromium, and 0.05% magnesium, with the remaining portion being

*Corresponding author e-mail: asfouda@hotmail.com.; (A.S. Fouda).
Receive Date: 08 June 2024, Revise Date: 24 June 2024, Accept Date: 09 July 2024
DOI: 10.21608/ejchem.2024.296213.9829

aluminum. The corrosive environment simulated was a 1 M hydrochloric acid (HCl) solution prepared by diluting concentrated analytical grade HCl (37%) with double the volume of purified distilled water. To assess the potential inhibition effect, a stock solution of yellow oleander extract (1000 ppm) was used. The desired inhibitor concentrations were obtained by further dilution with double-distilled water.

2.2. Plant Extract preparation

A powder with fine properties is prepared by grinding dried yellow bay flowers. The resulting powdered material, about 250 g, was soaked in 0.5 liters of dichloromethane for 120 hours and then periodically removed by 5 times 50 ml to extract the used plant material. After evaporating all the dichloromethane, a solid extract was obtained which was then prepared for use as a corrosion inhibitor. Chemical studies have shown that the main chemical components of yellow oleander are thevetin B, cannogenin, digoxigenin and cannonigenol [22].

2.3. ML method

Aluminum (Al) samples were pre-weighed and then immersed in 0.1 liters of 1 M HCl solution. The experiment investigated the effect of different YOE inhibitor concentrations, ranging from 50 ppm to 300 ppm. After various immersion times, the samples were removed, rinsed with double-distilled water, carefully dried, and weighed again with high precision. Based on the weight changes, the inhibition efficiency (IE %) and surface coverage (θ) of YOE on the aluminum surface were calculated [23].

$$"IE\% = \theta x\ 100 = \left[1 - \frac{W}{W^{\circ}}\right] x\ 100" \qquad (1)$$

where W^{o} and W are the average ML without and with the inhibitor, separately.

2.4. Electrochemical measurements

A standard three-electrode cell setup was used for the electrochemical measurements. This setup consisted of: Working electrode: A 1 cm² aluminum electrode. Prior to the experiment, this electrode was polished using 1200-grit sandpaper and then thoroughly rinsed with water to remove any surface impurities. Reference electrode: A saturated calomel electrode (SCE) served as the reference point for potential measurements. Counter electrode: A platinum foil acted as the counter electrode. The complete cell was immersed in 1 M HCl solution, which served as the aggressive electrolyte. It's important to note that all the tests were conducted at a controlled temperature of 25 °C.

PDP measurements were performed by scanning the potential ± 250 mV from E_{corr} at a scanning rate of 1 mV s^{-1} after the steady state of the working electrode had been reached (30 min) and an open circuit was obtained. Voltage (OCP). Measurements of EIS were performed over the frequency range (10^5 till 0.1 Hz) with a peak-to-peak gain of 10 mV using an AC signal at open-circuit potential. The most convincing parameters from inspection of the Nyquist plot are the charge transfer resistance (R_{ct}) and double layer capacitance (C_{dl}) characterized by:

$$C_{dl} = \frac{1}{2\pi f_{max} R_p} \qquad (2)$$

where f_{max} is the precise frequency at which the imaginary component of the impedance comes to its greatest values. The obstacle productivity and surface perimeter (θ) obtained from impedance estimation were characterized by the following equations:

$$\%\ IE = \left(1 - \frac{R_p^{\circ}}{R_p}\right) \times 100 \qquad (3)$$

where R_p and R^{o}_p are the polarization resistance within the presence and absence of the inhibitor, respectively.

Electrochemical Frequency Modulation (EFM) measurements were conducted at two frequencies: 2 and 5 Hz. Since the fundamental frequency is 0.1 Hz, this means the tip oscillation repeats ten times per second (1/0.1 Hz). The EFM data provides an intermodulation spectrum, which combines the current response from harmonic peaks (multiples of the fundamental frequency) and additional intermodulation currents. These peaks were used to determine key corrosion parameters, including the corrosion current density (i_{corr}), the Tafel slopes for both anodic (β_a) and cathodic (β_c) reactions, and specific causal factors represented by CF2 and CF3. It's important to note that the open circuit potential (OCP) likely stabilized within 30 minutes before these measurements began. The tests were performed at a room temperature of (25 ±1℃). All the measurements were done at least three times for reproducibility. Estimates were run using Gamry Instrument with the Gamry framework. In addition to Echem Analyst (version.5.03), the program is also used to plot and adjust the resulting data [24-26].

2.5. Surface morphology using SEM, AFM and EDX studies

For surface analysis, polished aluminum samples (dimensions 2.0 × 2.0 × 0.3 cm^3) were immersed in 1.0 M HCl containing inhibitor (YOE) at a maximum concentration of 300 ppm for 4 h at 25 °C. The samples were dried in fresh air in a desiccator and finally, two-dimensional SEM micrographs were taken using a JEOL JSM scanning electron microscope (Mansoura University). EDX tests were recorded in combination with SEM to determine the chemical composition in percentage of Al samples with and without YOE. Atomic force microscope (AFM) images were obtained using a FlexAFM3 model (Faculty of Engineering, Mansoura University).

3. Results and Discussion

3.1 ML Measurements

The loss in Al samples was calculated at different periods of time (T), in lack & existence of variant YOE concentrations, Figure (1). % IE is affected by YOE concentration. Curves of various YOE dosages can be found below the destructive media curve. Increasing the YOE concentration results in reduced mass loss and increased corrosion inhibition of aluminum. The ML results showed that YOE was considered an effective aluminum corrosion inhibitor in 1M HCl medium. Similarly, the surface coverage (***θ***) and inhibition efficiency increased by the increase of the concentration due to the light layer which is established by YOE adsorption [27]. Data produced from ML method were tabulated in Table (1).

Table (1): Variety of rate of corrosion (k_{corr}), coverage of surface (θ) and inhibitor efficiency (%IE) with various doses of YOE after 2h of dipping in 1M HCl at 25^{O}C.

[Inh]. ppm	**ML, mg cm^{-2}**	**k_{corr}, mg cm^{-2} min^{-1}**	**ϴ**	**%IE**
Blank	5.20	0.043333	-----	-----
50	1.69	0.014075	0.675	67.5
100	1.45	0.012054	0.722	72.2
150	1.22	0.010142	0.766	76.6
200	1.03	0.008588	0.802	80.2
250	0.83	0.006914	0.840	84.0
300	0.59	0.004902	0.887	88.7

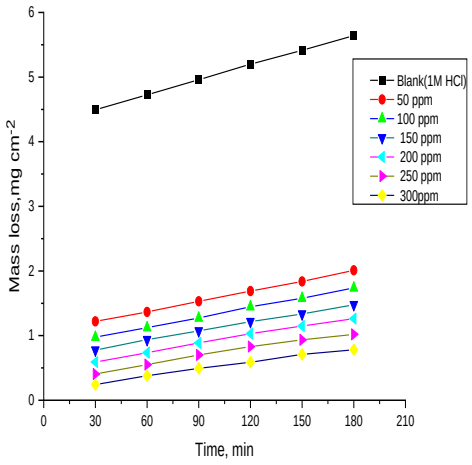

Figure 1: ML & T curve for Al corrosion 1M HCl in lack & presence of various concentrations of **YOE** at 25°C

3.2. Curves of PDP

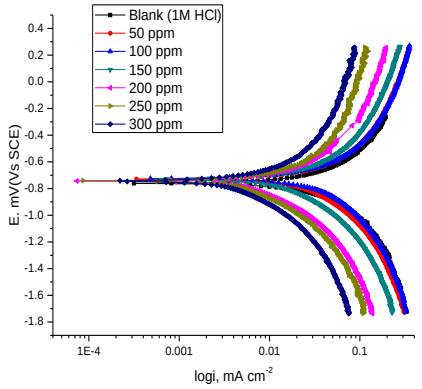

Figure 2: PDP charts for Al corrosion in 1M HCl solutions in the lack and the existence of diverse doses of YOE at 25ºC

Figure (2) shows polarization curves of Al corrosion in corrosive 1M HCl in the absence and presence of different YOE doses at room temperature.

The percentage of protection (%IE) and surface coverage (Θ) were calculated from equation (4)

$$\%IE = [(i^{o}_{corr} - i_{corr}) / i^{o}_{corr}] \times 100 = \theta \times 100 \quad (4)$$

"where i^{o}_{corr} and i_{corr} are the free and inhibited current densities, separately". As shown in Figure (2), both the anode and cathode are switched to a lower current density. Furthermore, the decrease in i_{corr} is clearly proportional to the increase in extract concentration, Table (2), demonstrating that the corrosion rate is reduced because the YOE layer is adsorbed and protects the Al surface from corrosion by HCl. The largest shift in corrosion potential (E_{corr}) by less than 85 mV suggests that YOE acts as a mixed-type inhibitor, i.e., influencing both oxidation (anodic) and reduction (cathodic) reactions at the metal surface [28]. Additionally, the unaltered Tafel slope implies that YOE primarily adsorbs on the metal, blocking active sites and hindering the corrosion process without altering the fundamental reaction mechanism [29].

Table (2): Corrosion potential (E_{Corr}), corrosion current density (i_{Corr}), Tafel slope (β_c, β_a), surface coverage (θ) and inhibitor efficiency (% IE) of Al in 1M HCl at 25°C.

$-E_{corr}$ mV vs SCE	i_{corr} m A Cm^{-2}	β_a mV dec^{-1}	$-\beta_c$ mV dec^{-1}	CRx10^3 mpy	Θ	%IE
761	276	251	421	163	---	---
722	137	152	172	59	0.504	50.4
727	127	80	100	57	0.540	54.0
729	108	71	95	51	0.609	60.9
735	96	60	91	44	0.652	65.2
737	82	54	83	37	0.703	70.3
739	71	31	70	11	0.743	74.3

.

3.3. Electrochemical Impedance Spectroscopy (EIS)

EIS was used to investigate the corrosion inhibition of Al by YOE after 30 minutes of immersion in 1 M HCl. Figure 3 displays the Nyquist plots, which reveal the impedance behavior of the Al electrode. These plots typically consist of a large loop at high frequencies (attributed to the relaxation process and dielectric properties of the native aluminum oxide layer) and a smaller loop at low frequencies (often associated with anodic adsorption intermediates influencing the oxidation process) [30-32]. It's important to note that the non-ideal semicircular shape of the loops likely arises from surface roughness and heterogeneity [33, 34]. Interestingly, the diameter of these loops increases with increasing YOE concentration (Figure 3). This trend suggests the adsorption of YOE on the Al surface and the formation of a protective film. Further evidence for this adsorption comes from the Bode plots in Figure 4. Here, we observe a rise in total impedance (Z) and a shift in the phase angle towards higher values with increasing YOE concentration, again supporting the notion of YOE adsorption on the Al surface [33-36]. To interpret the obtained impedance data, an equivalent circuit model is

presented in Figure 5. This demonstration includes "the solution resistance (R_s), the charge-transfer resistance of the interfacial corrosion reaction (R_{ct}), the inductance (L), the inductive resistance (R_L), and the double layer capacitance (C_{dl})". Through the results, this finding aligns well with the established principle that polarization resistance (R_p) can be determined for inductive circuits using the formula provided (Equation 5) [37]:

$$R_P = \frac{R_{ct} \times R_L}{R_{ct} + R_L} \qquad (5)$$

EIS data indicated that R_p values increased and C_{dl} values decreased with increasing YOE dose as in Table (3).This is usually due to the gradual replacement of H_2O atoms by the adsorption of extracted atoms on the metal surface and a decrease in the extent of decomposition reactions. High R_P values are mainly related to slower corrosion systems [38, 39].

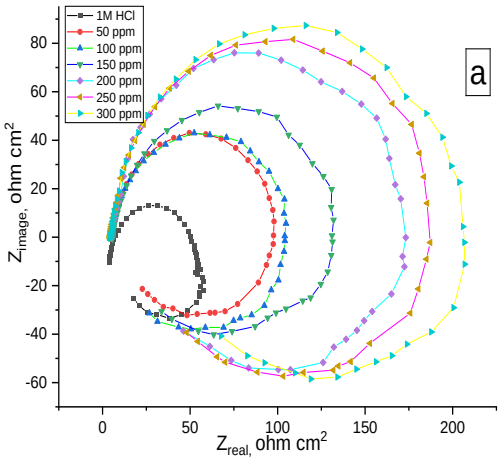

Figure 3: Nyquist plots for Al composite in 1 M HCl arrangements in the lack and existence of diverse concentrations of **YOE** at 25ºC.

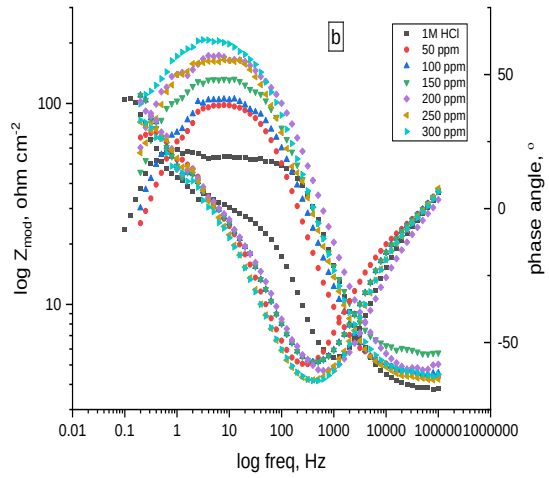

Figure 4: Bode plots for Al in 1 M HCl solutions in the lack & existence of diverse concentrations of **YOE** at 25ºC.

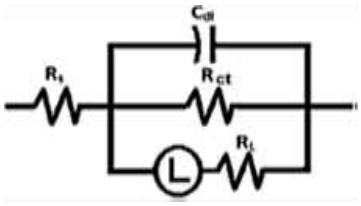

Figure 5: Electrical Circuit is established to fit impedance information

The decrease in C_{dl} may arise from a decrease in the adjacent dielectric constant and/or an increase in the thickness of the electric double layer [40], suggesting that the inhibitor molecules act by absorbing at the interface. Metal/solution. The %IE obtained from EIS measurements is close to the value found from PP measurements. %IE are calculated using the following equation (6):

$$\% IE = [1 - (R^o_p / R_p)] \times 100 = \theta \times 100 \qquad (6)$$

Table (3): Electrochemical parameters acquire from EIS technique for Al in 1 M HCl in the lack and existence of YOE diverse concentrations

[Inh]. ppm	R_{ct} Ω cm^2	*Cdl µFcm^{-2}*	R_L Ω cm^2	R_p, Ω cm^2	Ɵ	*%IE*
0	51.84	177.00	17.30	12.97	---	---
50	93.27	54.40	71.48	40.47	0.680	68.0
100	100.53	40.20	76.56	43.47	0.702	70.2
150	127.90	31.91	98.02	55.49	0.766	76.6
200	169.30	24.28	138.32	76.13	0.829	82.9
250	180.60	21.99	148.97	81.63	0.841	84.1
300	203.00	20.53	153.32	87.35	0.852	85.2

3.4. EFM Measurements

A safe damping method that detects corrosion current with only a small error signal without knowing the Tafel constant [41]. Figure (6) shows the EFM spectrum of Al in 1 M HCl solution at different YOE concentrations. From Table (4), adding YOE at different dosages to destructive medium reduced the density of corrosion current, these indicate that YOE adsorbed on the Al surface and formed a protective layer. A causal factor closes to the hypothetical quantity as stated in the EFM hypothesis [42] would prove the validity of the measurement. The % IE increases with increasing YOE concentration and tends to be evaluated according to equation (4).

.

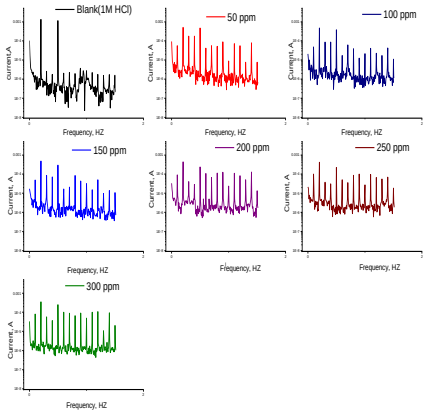

Figure 6: Intermodulation spectra for Al corrosion in 1 M HCl in lack and existence of diverse amount of YOE at 25˚C

Table (4): Electrochemical kinetic parameters acquired from EFM technique for Al in 1M HCl in the lack and existence of YOE diverse concentrations.

Inhibitor	[Inh]. ppm	i_{corr} µA Cm^{-2}	β_a mV dec^{-1}	$-\beta_c$ mV dec^{-1}	CF-2	CF-3	CRx10^{-3} mpy	Ɵ	*%IE*
Blank	Blank	51.84	177.00	17.30	1.4	2.2	670	---	---
Yellow Oleander Extract	50	93.27	54.40	71.48	1.9	2.6	240	0.680	68.0
	100	100.53	40.20	76.56	1.2	2.8	210	0.702	70.2
	150	127.90	31.91	98.02	1.8	2.3	202	0.766	76.6
	200	169.30	24.28	138.32	1.7	2.4	150	0.829	82.9
	250	180.60	21.99	148.97	1.3	2.6	146	0.841	84.1
	300	203.00	20.53	153.32	1.9	2.4	132	0.852	85.2

3.5. Adsorption Isotherm

Inhibitor Adsorption on metal surfaces has been extensively studied through the use of adsorption isotherms. The adsorption of organic molecules occurs due to the higher contact energy of the inhibitory metal surface than that of the aqueous metal surface [43-45]. To calculate the adsorption isotherm, the surface coverage (θ) was calculated from the ML method as a function of the

concentration of the inhibition function (C). The magnitude of θ was then plotted to represent the best-fitting adsorption model [46]. Numerous attempts have been performed to fit the experimental data to various isotherms such as the Frumkin isotherm, Langmuir isotherm, Temkin isotherm, and Freundlich isotherm. The obtained results were best matched with the Langmuir adsorption isotherm, as shown in figure (70) [47].

$$\theta /1 - \theta = K_{ads} C \qquad (7)$$

"where K_{ads} is the equilibrium adsorption constant, which is derived from the slope of the Langmuir adsorption isotherm and correlates with the adsorption free energy $\Delta G°_{ads}$ as follows::

$$K_{ads}=1/55.5 \exp^{- \Delta G°ads/RT} \qquad (8)$$

"where, 55.5 is the molar concentration of water in the solution in M^{-1}". Data are given in Table 5.
Plot of (ΔG^{o}_{ads}) vs Temperature (K) (Fig. 8) provides adsorption heat (ΔH^{o}_{ads}) & entropy (ΔS^{o}_{ads}) based on thermodynamic equation (9) as shown:

Table (5): The adsorption thermodynamic parameters for YOE on Al surface in 1 M HCl at various Temperatures

Inhibitor	**Temp. °C**	**K_{ads} ppm^{-1}**	**$-\Delta G^{o}_{ads}$ *k J mol^{-1}***	**$-\Delta H^{o}_{ads}$ k J mol^{-1}**	**$-\Delta S^{o}_{ads}$ J mol^{-1} k^{-1}**
Yellow Oleander Extract	25	25.88	18.02	54.894	123.76
	30	23.29	17.05		124.89
	35	19.25	16.66		124.13
	40	13.54	15.94		124.47
	45	6.25	15.47		123.99

$$\Delta G^{o}_{ads} = \Delta H^{o}_{ads} - T \Delta S^{o}_{ads} \qquad (9)$$

Table (5) clearly shows the excellent reliability of ΔG^{o}_{ads} with respect to T. The negative value of ΔG^{o}_{ads}

Suggests a favorable and spontaneous adsorption process for YOE on the aluminum surface. ΔG^{o}_{ads} values below about -20 kJ/mol are largely related to electrostatic interactions (physisorption) between the charged YOE molecules and the charged Al surface. However, values above about -40 kJ mol^{-1} are consistent with the YOE molecules sharing or transferring charge to the Al surface to form a kind of coordinate bond (chemisorption) [48]. Adsorption has been established physically from the Al surface. Data provided by ΔH^{o}_{ads} (from -15.47 to -18.02 kJ mol^{-1}). The promotion of endothermic adsorption ($\Delta H^{o}_{ads} > 0$) clearly depends on the chemisorption process [49], an exothermic process ($\Delta H^{o}_{ads} < 0$) that may involve chemisorption or
Physisorption or mix of both. ΔH^{o}_{ads} value determined here for the adsorption of yellow oleander in acidic solution demonstrates that this inhibitor can be chemically adsorbed onto the Al surface. The sign of ΔS^{o}_{ads} when YOE exists is negative, indicating that the disorder of the corrosion process on the Al surface is reduced [50].

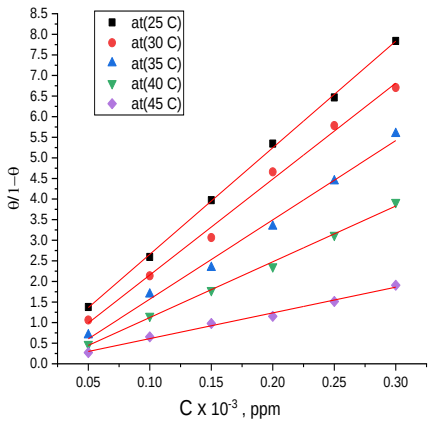

Figure 7: Curves of Langmuir adsorption for Al in 1M HCl + several doses of **YOE** at different temperatures.

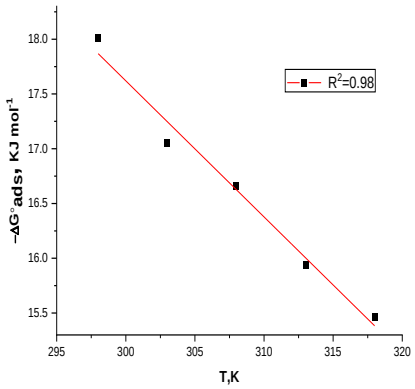

Figure 8: The Variety of ΔG^{o}_{ads} for **YOE** adsorption on Al surface in 1 M HCl at different temperatures

3.6. The corrosion thermodynamic parameters

The ML method was performed at different temperatures (25-45 °C) in the presence of different YOE concentrations. Higher temperatures led to a higher corrosion rate for the aluminum alloy in 1.0 M HCl, as shown in (Table 1). This trend translates to a decrease in the %IE (inhibition efficiency) of YOE with increasing temperature. (Table1) summarizes the corrosion parameters measured in the absence and presence of YOE at various temperatures (25 °C to 45 °C). Additionally, the Arrhenius equation was used to calculate the activation energy (Ea*) for aluminum alloy dissolution in 1.0 M HCl. Slope of the graph is:

$$\log k = \frac{-E_a^*}{2.303\,R\,T} + \log A \qquad (10)$$

"Where the rate of corrosion is expressed by k_{corr} and A is the Arrhenius pre-exponential factor". The E^*_a values calculated from the plot of log k_{corr} versus temperature are shown in Figure (9). The E^*_a values for Al in 1M HCl increase with increasing YOE concentration. It can be concluded that the presence of YOE forms an energy barrier to the corrosion reaction and this barrier increases with increasing extractive concentration. Therefore, the protective effect of the extractives decreased significantly with increasing temperature. This result indicates that adsorption of YOE particles on Al alloy surface is considered to be a physical adsorption [51]. Entropy change (ΔS^*) & enthalpy change (ΔH^*) shall be calculated as shown:

$$k_{corr} = \left(\frac{RT}{Nh}\right) exp\left(\frac{\Delta S^*}{R}\right) exp\left(\frac{\Delta H^*}{RT}\right) \qquad (11)$$

"where k is the rate of corrosion, h is Planck's constant, N is Avogadro number, ΔS^* is the entropy of activation, and ΔH^* is the enthalpy of activation". A graph of log (k/T) versus 1/T (Figure 10) gives a line with a slope of (ΔH^*/2.303R) and an intercept of [log (R/Nh) +ΔS^*/2.303R]. The magnitude of ΔS^* and ΔH^* can be calculated (Table 6).

The magnitude ΔS^* is -ve, indicating that the complex is activated during the rate-determining step representing association rather than the dissociation stage [52]. Sign for ΔH^* is +ve, indicating that the adsorption is an endothermic process. Usually, endothermic process means chemical adsorption process.

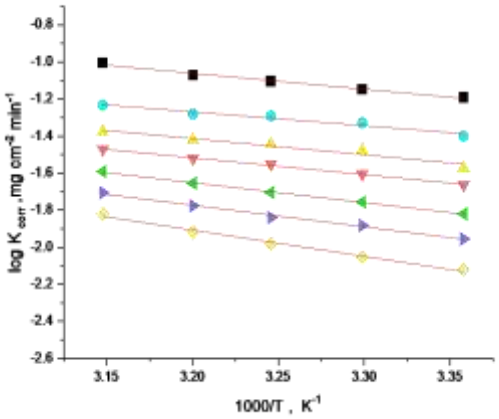

Figure 9: Arrhenius plots for aluminum corrosion rates (k_{corr}) after 120 minutes of dipping in 1 M HCl with and without different concentrations of Yellow Oleander extract.

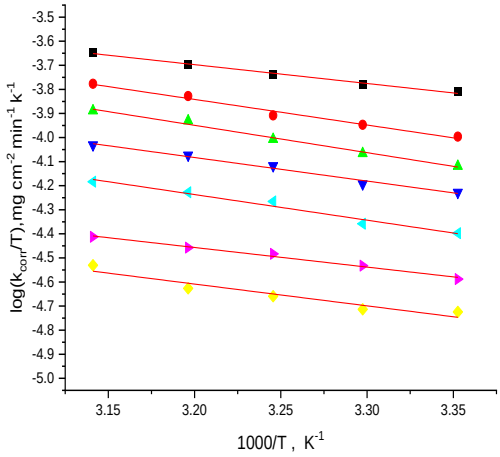

Figure 10: Transition-state For Al corrosion in 1M HCl without and with diverse concentrations of Yellow Oleander extract.

Table (6): Parameters thermodynamic activation for corrosion of Al in lack & existence of variant amount of YOE in 1M HCl.

Conc. ppm	E_a^*, kJ mol^{-1}	ΔH^*, kJ mol^{-1}	$-\Delta S^*$, J mol^{-1}K^{-1}
Blank	16.5	15.0	213.4
50	14.3	15.6	232.9
100	16.7	17.3	230.2
150	17.3	15.0	220.3
200	22.7	20.4	205.9
250	24.4	21.7	203.5
300	27.1	24.2	215.7

3.7. SEM analysis

Surface morphology studies were performed on the surface of the Al coupon before dipping it in 1.0 M HCl solution (free Al sample) [Fig.11(a)] and after immersing it in 1.0 M HCl without adding YOE [Fig.11(b)] and with addition of the highest concentration of inhibitor (300 ppm) [Fig.11(c)] for 4 h. Significant degradation was observed on the Al surface in 1.0 M HCl solution [Fig.11(b)], with large pauses; Grooves which are appearing on entire Al surface clearly illustrate a high rate of corrosion.

[Fig. 11(a)] shows an image of a free Al coupon with a uniformly flat surface. After 4 h of immersion, the sample surface (Al) was significantly protected by the inhibitor YOE [Fig. 11(c)], which shows a flat surface without any cracks or holes, indicating a significant reduction in corrosion. Furthermore, in the presence of inhibitor, it was observed that layer formation occurs due to the adsorption of YOE molecules into a thick coating layer. Therefore, it can be concluded that YOE acts as a very effective corrosion inhibitor through its adsorption onto the Al surface in 1.0 M HCl solution [53].

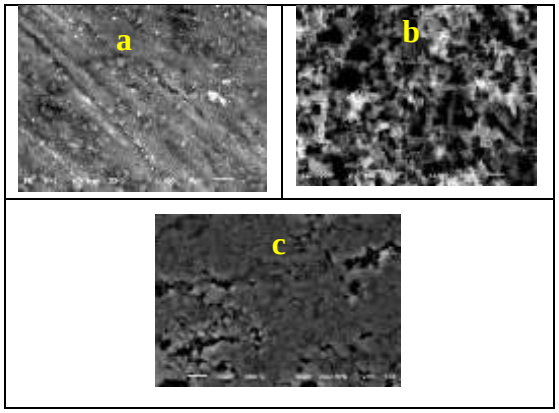

Figure 11: SEM images of (a) Free Al surface, (b) Al in 1.0 M HCl, (c) Al in 1.0 M HCl +300 ppm YOE, after 4 h exposure at the ×1000 magnification.

3.8 AFM analysis

This analysis is considered to be an important test for determining the roughness of Al metal surfaces at the highest resolution in nano scaling [54]. The technique provides information about surface shape of Al, which is useful for scientific research in corrosion. The three-dimensional AFM image is shown in Fig.12. Average roughness (Ra) is illustrated in Table 7. A relative perspective scale view in Table 7 clearly shows that the metal surface before immersion in smoothed HCl acid (4.3 nm), then dipped in 1 M HCl, the surface was destroyed, and roughness increased (10.4 nm) while the Al sample which is dipped in 300 ppm YOE its surface became smoother and less roughness (5.4 nm) compared to the blank sample due to adsorption. A protective film of YOE is formed on the Al metal surface.

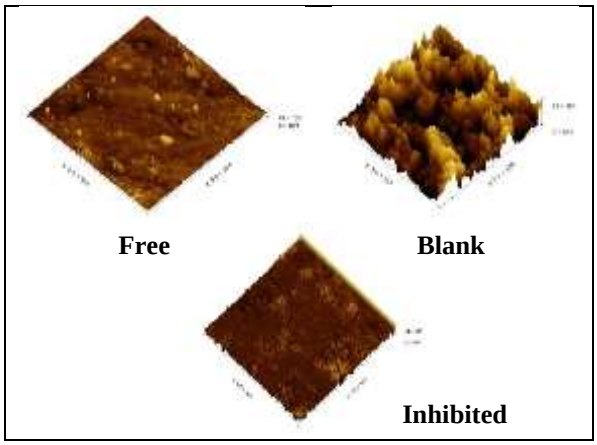

Figure 12: 3-D AFM images of Al metal before dipping into 1 M HCl (free) and after dipping in 1 M HCl in the absence (blank) and presence of 300 ppm of **YOE** (inhibited) for 24 h at 25℃.

Table (7): AFM roughness data of Yellow Oleander at 300 ppm for 24 h at 25ºC

Al Sample	The Average Roughness (R_a) x 10^{-9}
Free – Al Surface	4.3
Blank- Al dipped in 1M HCl	10.4
Al dipped in (1M HCl + 300 ppm YOE)	5.4

3.8 EDX technique

An attempt was made to analyze Al surfaces by performing energy dispersive X-ray spectroscopy in lack of Yellow Oleander Extract (YOE). The SEM image of an Al coupon immersed in 1.0 M 300 ppm YOE HCl solution stored at room temperature is shown in Figure 11(b) and the corresponding EDX spectrum is shown in Figure 13(b). The spectrum in Figure 13(a) shows aluminum and oxygen peaks, indicating the formation of aluminum oxide/hydroxide on the Al sample surface.

All other data indicate that the presence of YOE molecules significantly reduces the formation of aluminum oxide, thus resulting in a lower oxygen content on the Al surface, and these compounds act as good Al corrosion protection. There are high intensity peaks due to the presence of conjugated heterocyclic ring, carbon and oxygen, which clearly shows the adsorption capacity of YOE molecule on Al sample [55, 56].

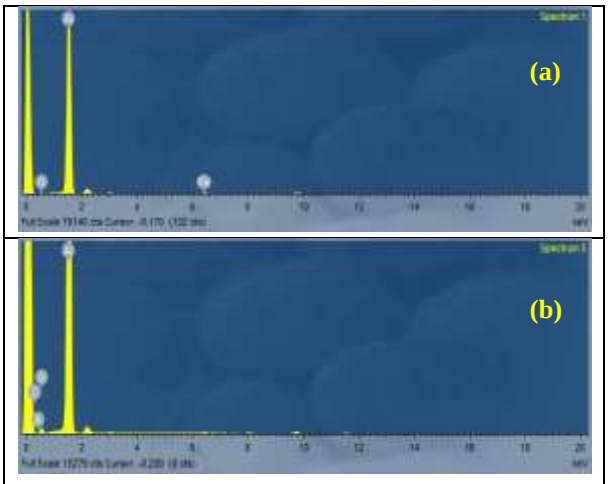

Figure 13: EDX spectra of (a) Blank Al surface in 1.0 M HCl, (b) Al in 1.0 M HCl + 300 ppm YOE

3.9. Mechanism of the corrosion inhibition

YOE effectively prevents aluminum corrosion, as confirmed by both chemical and electrochemical analyses. The mechanism appears to involve blocking the adsorption sites for competing surfactants, allowing YOE to form a protective layer on the metal surface [57, 58]. This protective layer formation is attributed to YOE's physical adsorption. The low ΔG^{o}_{ads} value (around 14 $kJmol^{-1}$) suggests weak electrostatic interactions between the negatively charged aluminum surface and positively charged components of protonated YOE. Additionally, the presence of C=O, OH groups, and π-electrons in the benzene ring of YOE molecules likely contribute to their adsorption on the aluminum surface [59-60]

4. Conclusion

Multiple analysis techniques, including chemical, electrochemical, and surface science methods were used to confirm the effectiveness of the extract towards the corrosion of Al in HCl solution. The PDP curves indicate that YOE acts as a mixed-type inhibitor by hindering both oxidation (anodic) and reduction (cathodic) reactions on the Al surface. Interestingly, the effectiveness of YOE (inhibition efficiency) weakens as the temperature rises. Further investigation revealed that YOE adsorbs onto the Al surface through a physical adsorption process that follows the Langmuir isotherm model. This adsorption mechanism was corroborated by Atomic Force Microscopy (AFM) and Scanning Electron Microscopy (SEM) analysis. These microscopic techniques provided details about the Al surface's morphology (shape and features), roughness, and any chemical interactions between YOE and the Al. The strong agreement between the chemical and electrochemical measurements reinforces the conclusion that YOE effectively adsorbs onto the Al surface.

.

References

1. Trabanelli, G. (1991). Corrosion, 47(6), 410-419.
2. Singh, D., & Dey, A. (1993). Corrosion, 49(7), 594 600.
3. Banerjee, G., & Malhotra, S. (1992). Corrosion, 48(1), 10-15.
4. Arab, S. T., & Noor, E. A.-a. (1993). Corrosion, 49(2), 122-129.
5. Raspini, I. (1993). Corrosion, 49(10), 821-828.
6. Khadraoui, A., Khelifa, A., Touafri, L., Hamitouche, H., & Mehdaoui, R. (2013). J. Mater. Environ. Sci, 4(5), 663-670.
7. Elachouri, M., Hajji, M., Kertit, S., Essassi, E., Salem, M., & Coudert, R. (1995). Corrosion Science, 37(3), 381-389.
8. Luo, H., Guan, Y., & Han, K. (1998). Corrosion, 54(08).
9. Migahed, M., Azzam, E., & Al-Sabagh, A. (2004). Materials Chemistry and Physics, 85(2-3), 273-279.
10. Villamil, R. F., Corio, P., Agostinho, S. M., & Rubim, J. C. (1999). Journal of Electroanalytical chemistry, 472(2), 112-119.
11. Kumar, S. H., & Karthikeyan, S. (2012). J. Mater. Environ. Sci, 3(5), 925-934.
12. Fouda, A., Abou-shahba, R., Husien, W., & EL-Habab, E. (2016). J. Mater. Environ. Sci, 1(4), 227-238.
13. Abd El Rehim, S. S., Hassan, H. H., & Amin, M. A. (2003). Materials Chemistry and Physics, 78(2), 337-348.
14. Guo, R., Liu, T., & Wei, X. (2002). Colloids and Surfaces A: Physicochemical and Engineering Aspects, 209(1), 37-45.
15. Branzoi, V., Golgovici, F., & Branzoi, F. (2003). Materials Chemistry and Physics, 78(1), 122-131.
16. Parikh, K., & Joshi, K. (2004). Trans. SAEST, 39, 29-35.
17. Healy, B. M. (2022). Orient Journal of Chemistry, 30 (1) 3760.
18. Ali, A., & Foaud, N. (2012). J. Mater. Environ. Sci, 3(5), 917-924.
19. Nwosu, O., Osarolube, E., Nnanna, L., Akoma, C., & Chigbu, T. (2014). American journal of Materials science, 4(4), 178-183.
20. James, A., & Akaranta, O. (2009). African Journal of Pure and Applied Chemistry, 3(12), 262-268.
21. Yarkasuwa, C. I., Wilson, D., & Michael, E. (2013). Journal of the Korean Chemical Society, 57(3), 377-381.
22. Hase, G. J., Deshmukh, K. K., Pokharkar, R. D., Gaje, T. R., & Phatanagre, N. D. (2017). International Journal of Pharmacognosy and Phytochemical Research, 9(6), 885-891.
23. El-Shamy, A. M., & Abdel Bar, M. M. (2021). *Egyptian Journal of Chemistry*, *64*(4), 1867-1876.
24. Onuchukwu, A., & Adamu, A. (1990). Materials Chemistry and Physics, 25(3), 227-235.
25. El Sheikh, M., El Hassan, G., Hafeez, A.-R. E. T. A., Abdalla, A., & Antoun, M. (1982). Planta medica, 45(06), 116-119.
26. Eeva, M., Salo, J.-P., & Oksman-Caldentey, K.-M. (1998). Journal of Pharmaceutical and biomedical analysis, 16(5), 717-722.
27. Mu, G., P Zhao, T., Liu, M., & Gu, T. (1996). Corrosion, 52(11).
28. Parr, R. G., Donnelly, R. A., Levy, M., & Palke, W. E. (1978). The Journal of chemical physics, 68(8), 3801-3807.
29. Bosch, R., Hubrecht, J., Bogaerts, W., & Syrett, B. (2001). Corrosion, 57(1), 60-70.
30. Zhang, D.-Q., Cai, Q.-R., He, X.-M., Gao, L.-X., & Kim, G. S. (2009). Materials Chemistry and Physics, 114(2-3), 612-617.
31. Lee, H., & Nobe, K. (1986). Journal of the Electrochemical Society, 133(10), 2035.
32. Tao, Z., Zhang, S., Li, W., & Hou, B. (2009). Corrosion Science, 51(11), 2588-2595.
33. Ferreira, E., Giacomelli, C., Giacomelli, F., & Spinelli, A. (2004). Materials Chemistry and Physics, 83(1), 129-134.
34. Abdel-Fatah, H. T., Kamel, M. M., Hassan, A. A., Rashwan, S. A., Abd El Wahaab, S. M., & El-Sehiety, H. E. (2017). Arabian Journal of Chemistry, 10, S1164-S1171.
35. Growcock, F., & Jasinski, R. (1989). Journal of the Electrochemical Society, 136(8), 2310.
36. Abdel–Rahim, S., Khaled, K., & Abd–Elshafi, N. (2006). Electrochim. Acta, 51(16), 3269-3377.
37. Megahed, M. M., Abdel Bar, M. M., & El-Shamy, A. M. (2021). *Egyptian Journal of Chemistry*, *64*(10), 5693-5702.
38. Caprani, A., Epelboin, I., Morel, P., & Takenouti, H. (1975). Inhibitors: Ferrara, Italy, 571.
39. Bessone, J., Mayer, C., Jüttner, K., & Lorenz, W. (1983). Electrochimica Acta, 28(2), 171-175.

40. Epelboin, I., Keddam, M., & Takenouti, H. (1972). Journal of applied electrochemistry, 2(1), 71-79.
41. Benedeti, A., Sumodjo, P., Nobe, K., Cabot, P., & Proud, W. (1995). Electrochimica Acta, 40(16), 2657-2668.
42. Ma, H., Chen, S., Niu, L., Zhao, S., Li, S., & Li, D. (2002). Journal of applied electrochemistry, 32, 65-72.
43. Li, X.-H., Deng, S.-D., & Fu, H. (2010). Journal of applied electrochemistry, 40, 1641-1649.
44. Lagrenee, M., Mernari, B., Bouanis, M., Traisnel, M., & Bentiss, F. (2002). Corrosion Science, 44(3), 573-588.
45. Kuş, E., & Mansfeld, F. (2006). Corrosion Science, 48(4), 965-979.
46. Caignan, G. A., Metcalf, S. K., & Holt, E. M. (2000). Journal of chemical crystallography, 30, 415-422.
47. Abdel-Rehim, S., Khaled, K., & Abd-Elshafi, N. (2006). Electrochimica Acta, 51(16), 3269-3277.
48. Bockris, J. M., & Swinkels, D. (1964). Journal of the Electrochemical Society, 111(6), 736.
49. Lorenz, W., & Mansfeld, F. (1981). Corrosion Science, 21(9-10), 647-672.
50. Yurt, A., Bereket, G., Kivrak, A., Balaban, A., & Erk, B. (2005). Journal of applied electrochemistry, 35, 1025-1032.
51. Sastri, V., Elboujdaini, M., Brown, J., & Perumareddi, J. (1996). Corrosion, 52(6), 447-452.
52. Hamdani, N. E., Fdil, R., Tourabi, M., Jama, C., & Bentiss, F. (2015). Appl Surf Sci, 357(Part A), 1294-1305.
53. Singh, P., Srivastava, V., & Quraishi, M. (2016). Journal of Molecular Liquids, 216, 164-173.
54. Gao, X., Liu, S., Lu, H., Gao, F., & Ma, H. (2015). Industrial & Engineering Chemistry Research, 54(7), 1941-1952.
55. Droulas, J., Duc, T. M., & Jugnet, Y. (1991). Le vide, les couches minces, 258, 39-41.
56. Kovac C.A., Clabes J.G, Goldberg. M.J , Vac. J. Sci. Technol., A 6 (1988) 991
57. Gu, T., Chen, Z., Jiang, X., Zhou, L., Liao, Y., Duan, M., Wang, H., & Pu, Q. (2015). Corrosion Science, 90, 118-132.
58. Yadav, M., S. Kumar, R. Sinha, I. Bahadur and E. Ebenso (2015). Journal of Molecular Liquids 211: 135-145.
59. Goyal, M., Vashisht, H., Kumar, S., & Bahadur, I. (2018). Journal of Molecular Liquids, 261, 162-173.
60. Le Mehaute, A., & Crepy, G. (1983). Solid State Ionics, 9, 17-30